

On the Backbending Mechanism of ^{48}Cr

Kenji Hara⁽¹⁾, Yang Sun⁽²⁾ and Takahiro Mizusaki⁽³⁾

⁽¹⁾Physik-Department, Technische Universität München, D-85747 Garching, Germany

⁽²⁾Department of Physics and Astronomy, University of Tennessee, Knoxville, TN 37996, USA

⁽³⁾Department of Physics, University of Tokyo, Hongo, Tokyo 113, Japan

The mechanism of backbending in ^{48}Cr is investigated in terms of the Projected Shell Model and the Generator Coordinate Method. It is shown that both methods are reasonable shell model truncation schemes. These two quite different quantum mechanical approaches lead to a similar conclusion that the backbending is due to a band crossing involving an excited band which is built on simultaneously broken neutron and proton pairs in the “intruder” subshell $f_{7/2}$. It is pointed out that this type of band crossing is usually known to cause the second backbending in rare-earth nuclei.

PACS: 21.60.Cs, 21.60.Ev, 23.20.Lv, 27.40.+z

Investigation of the yrast band in the ^{48}Cr nucleus has recently become a particularly interesting subject in nuclear structure studies because of the full pf -shell model calculation [1] on the one hand and of the spectroscopic measurements [2,3] on the other. It is a light nucleus for which an exact shell model diagonalization is feasible, yet exhibits remarkable high-spin phenomena usually observed in heavy nuclei: large deformation, typical rotational spectrum and the backbending in which regular rotational spectrum is disturbed by a sudden irregularity at a certain spin. This nucleus is therefore an excellent example for theoretical studies, providing a unique testing ground for various approaches.

The intrinsic and laboratory frame descriptions of this nucleus were presented in a paper by the Strasbourg-Madrid collaboration [1]. These approaches are complementary views of the same problem from two extremes. On the one hand, the cranked Hartree-Fock-Bogoliubov (CHFB) description interprets the problem in terms of the intrinsic frame on which the lowest rotational band (yrast band) is built. It can provide a nice physical insight but does not treat the angular momentum as a good quantum number. On other hand, the pf -shell model (pf-SM) approach solves the problem fully quantum mechanically and provides the exact solution of the Hamiltonian within the pf -shell. However, in the pf-SM, a single shell model configuration does not correspond to any excitation mode of deformed nucleus and therefore millions of many-body basis states are necessary even to represent the lowest eigenstate of the Hamiltonian. Consequently, the physical insight is lost and interpretation of the result becomes very difficult. The purpose of the present work is to clarify the physics associated with the yrast spectrum of the nucleus ^{48}Cr from two different quantum mechanical view points.

To extract physics, it is desirable to use a shell model basis which has a good classification scheme in the sense that a simple configuration corresponds (approximately) to a low excitation mode of the nucleus. This suggests us to use a deformed basis corresponding to the optimal set of basis states. In fact, a basis truncation can be most

easily done by selecting low-lying states if a proper deformed basis is used. To carry out a shell model type calculation with such a basis, the broken rotational symmetry (and the particle number conservation if necessary) has to be restored. This can be done by using the projection method to form a many-body basis in the laboratory frame. After this procedure, one diagonalizes the Hamiltonian. Such an approach lies conceptually between the two extreme methods mentioned above and takes the advantages of both. This is exactly the philosophy on which the Projected Shell Model (PSM) [4] is based.

The PSM uses the Nilsson+BCS representation as the deformed quasiparticle (qp) basis. Before performing a calculation for ^{48}Cr , one has to find out where the optimal basis is. The experimental lifetime measurement [3] suggests an axially symmetric deformation of $\beta \approx 0.28$ near the ground state of ^{48}Cr , which roughly corresponds to $\varepsilon_2 = 0.25$. We simply take this information and build our shell model basis at this deformation.

The set of multi-qp states relevant for our shell model configuration space is

$$|\Phi_\kappa\rangle = \{ |0\rangle, a_{\nu_1}^\dagger a_{\nu_2}^\dagger |0\rangle, a_{\pi_1}^\dagger a_{\pi_2}^\dagger |0\rangle, a_{\nu_1}^\dagger a_{\nu_2}^\dagger a_{\pi_1}^\dagger a_{\pi_2}^\dagger |0\rangle\}, \quad (1)$$

where a^\dagger 's are the qp creation operators, ν 's (π 's) denote the neutron (proton) Nilsson quantum numbers which run over properly selected (low-lying) orbitals and $|0\rangle$ the Nilsson+BCS vacuum or 0-qp state.

As in the usual PSM calculations, we will use the Hamiltonian [4]

$$\hat{H} = \hat{H}_0 - \frac{1}{2}\chi \sum_\mu \hat{Q}_\mu^\dagger \hat{Q}_\mu - G_M \hat{P}^\dagger \hat{P} - G_Q \sum_\mu \hat{P}_\mu^\dagger \hat{P}_\mu, \quad (2)$$

where \hat{H}_0 is the spherical single-particle Hamiltonian which in particular contains a proper spin-orbit force, whose strengths (i.e. the Nilsson parameters κ and μ) are taken from Ref. [5]. The second term in the Hamiltonian is the Q-Q interaction and the last two terms the monopole and quadrupole pairing interactions, respectively. It was shown [6] that these interactions simulate the essence of the most important correlations in nuclei,

so that even the realistic force has to contain at least these components implicitly in order for it to work successfully in the structure calculations. The interaction strengths are determined as follows: the Q-Q interaction strength χ is adjusted by the self-consistent relation such that the input quadrupole deformation ε_2 and the one resulting from the HFB procedure coincide with each other [4]. The monopole pairing strength G_M is taken to be $G_M = [22.5 - 18.0(N - Z)/A]/A$ for neutrons and $G_M = 22.5/A$ for protons, which was first introduced in Ref. [7]. This choice of G_M seems to be appropriate for the single-particle space employed in the present calculation in which three major shells ($N = 1, 2, 3$) are used for both neutron and proton. Finally, the quadrupole pairing strength G_Q is assumed to be proportional to G_M , the proportionality constant, which is usually taken in the range of 0.16 – 0.20, being fixed to 0.20 in the present work.

The eigenvalue equation of the PSM for a given spin I takes the form [4]

$$\sum_{\kappa'} \{H_{\kappa\kappa'}^I - E^I N_{\kappa\kappa'}^I\} F_{\kappa'}^I = 0, \quad (3)$$

where the Hamiltonian and norm matrix elements are respectively defined by

$$H_{\kappa\kappa'}^I = \langle \Phi_{\kappa} | \hat{H} \hat{P}_{KK'}^I | \Phi_{\kappa'} \rangle, \quad N_{\kappa\kappa'}^I = \langle \Phi_{\kappa} | \hat{P}_{KK'}^I | \Phi_{\kappa'} \rangle, \quad (4)$$

and \hat{P}_{MK}^I is the angular momentum projection operator. The expectation value of the Hamiltonian with respect to a “rotational band κ ” $H_{\kappa\kappa}^I/N_{\kappa\kappa}^I$ is called a band energy. When they are plotted as functions of spin I , we call it a band diagram [4]. It will provide us a useful tool for interpreting the result.

We have carried out not only the PSM calculation but also a calculation based on the Generator Coordinate Method (GCM) [8] with the same Hamiltonian as used in the pf-SM [1]. This is because the PSM Hamiltonian is quite schematic as it stands, so that we felt it necessary to confirm the result by another theory. The relation between the PSM and GCM will be discussed later. We will first explain briefly how the GCM is performed.

For given quadrupole moment q_{μ} and spin I , we look for the minimum of

$$\langle \hat{H}' \rangle \equiv \langle \hat{H} \rangle + c_1 \sum_{\mu=0,\pm 2} (\langle \hat{Q}_{\mu} \rangle - q_{\mu})^2 + c_2 [\langle \hat{J}_x \rangle - \sqrt{I(I+1)}]^2 \quad (5)$$

where c_1 and c_2 are predefined positive constants. This procedure generates a constrained Hartree-Fock (CHF) state $|q, \gamma, I\rangle$, where

$$q_0 = \sqrt{\frac{5}{4\pi}} q \cos \gamma, \quad q_{\pm 2} = \sqrt{\frac{5}{8\pi}} q \sin \gamma. \quad (6)$$

It is useful to plot an energy surface $\langle q, \gamma, I | \hat{H} | q, \gamma, I \rangle$ in the $q\gamma$ plane for each I , which usually shows several local minima. It will help us interpreting the result as we will soon see. We then project such Slater determinants corresponding to various q and γ onto a good angular momentum I and diagonalize the Hamiltonian with them, the eigenvalue equation being again of the form Eq.(3) with $|\Phi_{\kappa}\rangle = \{|q, \gamma, I\rangle\}$. The total number of mesh points in the $q\gamma$ parameter space is 66 in the present calculation, so that the size of the eigenvalue equation for a given spin I is at most $66 * (2I + 1)$ (some of them will be discarded due to vanishing norm). This is another way of truncating the shell model basis [8].

In Fig. 1, the results of the PSM and GCM for the γ -ray energy $E_{\gamma} = E(I) - E(I-2)$ along the yrast band, together with that of the pf-SM reported in Ref. [1], are compared with the newest experimental data [3]. One sees that four curves are bunched together over the entire spin region, indicating an excellent agreement of three theories with each other and with the data. The sudden drop in E_{γ} occurring around spin 10 and 12 corresponds to the backbending in the yrast band of ^{48}Cr .

In Fig. 2, three theoretical results for B(E2) are compared with the data [3]. Again, one sees that theories agree not only with each other but also with the data quite well. The B(E2) values decrease monotonously after spin 6 (where the first band crossing takes place in the PSM, see Fig. 3 and discussions below). This implies a monotonous decrease of the intrinsic Q-moment as a function of spin, reaching finally the spherical regime at higher spins. This feature was explicitly discussed in Ref. [1] within the CHFB framework.

Figs. 1 and 2 indicate that both PSM and GCM are reasonable shell model truncation schemes as they reproduce the result of the pf-SM very well. Let us study their band diagrams to understand why and how the backbending occurs. As mentioned before, a band diagram displays band energies of various configurations before they are mixed by the diagonalization procedure Eq.(3). It can provide a transparent picture of band crossings. Irregularity in a spectrum may appear if a band is crossed by another one at certain spin. We remark in this connection that a small crossing angle implies a smooth change in the yrast band while a large crossing angle a sudden change, leading to a backbending [9].

In Fig. 3, the band diagram of the PSM is shown. Different configurations are distinguished by different types of lines, and the filled circles represent the yrast states obtained after the configuration mixing. Among several 2-qp bands which start at energies of 2 – 3 MeV, two of them (one solid and another dashed line) cross the ground band at spin 6. They are neutron 2-qp and proton 2-qp bands consisting of two $f_{7/2}$ quasiparticles of $\Omega = 3/2$ and 5/2 coupled to total $K = 5/2 - 3/2 = 1$ forming the so-called s -band. The crossing angle is relatively small so that the yrast band smoothly changes its structure

from the 0-qp to the 2-qp states around spin 6. Therefore, no clear effect of this (first) band crossing is seen in the yrast band (cf. Fig. 1). These $\Omega = 3/2$ and $5/2$ Nilsson states are nearly spherical in which the $j = 7/2$ component dominates (95% and 98% respectively). This is nothing other than the property which characterizes the intruder states.

The above two ($K = 1$) 2-qp bands can combine to a ($K = 2$) 4-qp band which represents simultaneously broken neutron and proton pairs. In Fig. 3, this 4-qp band (one of the dashed-dotted lines which becomes the lowest band for $I \geq 10$) shows a unique behavior as a function of spin. As spin increases, it goes down first but turns up at spin 6. This behavior has its origin in the spin alignment of a decoupled band as intensively discussed in Ref. [4]. Because of this, it can sharply cross the 2-qp bands between spin 8 and 10 and becomes the lowest band thereafter, so that the yrast band gets the main component from this 4-qp band. This is seen in the band diagram as a (second) band crossing. Thus, we can interpret the backbending in ^{48}Cr as a consequence of the simultaneous breaking of the $f_{7/2}$ neutron and proton pairs.

Similar band crossing picture emerges also from the band diagram of the GCM (here we use the word “band” symbolically). In Fig. 4, two most prominent bands in the GCM are shown together with the yrast band obtained after the diagonalization. The one labelled as deformed band is associated with a prolate minimum while the one labeled as spherical band with the zero deformation which becomes a minimum only when spin is higher. Fig. 4 shows the competition between these two bands which are built by diagonalizing the Hamiltonian within small regions of the $q\text{-}\gamma$ plane around the respective local minima in the energy surface. Therefore, in the GCM, the backbending in ^{48}Cr can be interpreted as due to the crossing between the deformed and spherical band. The latter dominates beyond spin 10 and this explains the sudden decrease of the Q-moment in the pf-SM calculation.

While the deformed band in the GCM corresponds obviously to an admixture of the 0-qp and a 2-qp band in the PSM, we note that the feature of the spherical band in Fig. 4 looks similar to that of the 4-qp band in Fig. 3. In fact, the 4-qp band of the PSM can be considered as a spherical band because the main part of its wavefunction is a product of the $j = 7/2$ components as mentioned before, while the spherical band of the GCM can be thought as the 4-qp band because it consists mainly of the $f_{7/2}$ neutrons and protons as its occupation number indicates. Thus, we have the same physics in two different languages and may conclude that the backbending of ^{48}Cr is due to the band crossing caused by a simultaneous neutron and proton pair breaking in the $f_{7/2}$ shell. We remark that this statement differs completely from that of a recent paper [10] based on the CHFB which claims that

the backbending in ^{48}Cr is not due to band crossing.

To conclude, both PSM and GCM are reasonable shell model truncation schemes and suggest consistently that the backbending of ^{48}Cr is due to a band crossing. The PSM carries out the configuration mixing in terms of qp-excitations while the GCM in terms of Slater determinants that belong to different nuclear shapes. We have shown in the present context that they describe the same physics. However, in the PSM terminology, the backbending in ^{48}Cr is not due to the crossing between the 0-qp and 2-qp band (or the so-called $g\text{-}s$ band crossing) but rather to the one between a 2-qp and 4-qp band. This is remarkable because such a band crossing is known to lead to the second backbending in rare-earth nuclei [9]. The $g\text{-}s$ band crossing which usually leads to the first backbending shows no prominent effect in ^{48}Cr except for the decrease in $B(E2)$ values. This is because the spin alignment of a 2-qp band cannot become large enough in light nuclei as the maximal value is limited to $J = 6$ in the intruder subshell $f_{7/2}$, which is only the half of what is possible ($J = 12$) in the intruder subshell $i_{13/2}$ of rare-earth nuclei.

One basic question still remains. The PSM uses a schematic Hamiltonian while the GCM the same realistic Hamiltonian as the pf-SM. How can the PSM deliver a similar result as the latter two? The answer to this question was actually given in Appendix B of Ref. [4]. It was proved that the band energies do not depend on details of the Hamiltonian for the ground and intruder bands of a well deformed system and that any (rotation invariant) Hamiltonian, which gives similar values for (1) the fluctuation of the angular momentum, (2) the Peierls-Yoccoz moment of inertia and (3) the qp excitation energies, will lead essentially to the same result. The first two conditions are the ground state properties that determine the scaling of a band diagram while the last one the relative position of various bands reflecting the shell filling of the nucleus in question. The detailed spin dependence such as the signature rules (for example, even/odd spins are favoured/unfavoured in an even-even system) originate solely from the kinematics of angular momenta. Note that the yrast band is essentially the envelope of the band energies as one can see in Fig. 3. This explains the reason why the PSM works so nicely even with a simple schematic Hamiltonian.

The present work is supported in part by Grant-in-Aid for Scientific Research (A)(2)(10304019) from the Ministry of Education, Science and Culture of Japan. K.H. and Y.S. acknowledge A.P. Zuker for a conversation made during the *Drexel Shell Model Workshop* in Philadelphia, 1996, stimulating them to carry out a PSM analysis [11] of the nucleus ^{48}Cr on which a part of the present work is based.

- [1] E. Caurier, J.L. Egido, G. Martínez-Pinedo, A. Poves, J. Retamosa, L.M. Robledo, and A.P. Zuker, Phys. Rev. Lett. **75**, 2466 (1995)
- [2] J.A. Cameron, *et al*, Phys. Lett. **B387**, 266 (1996)
- [3] F. Brandolini, *et al*, Nucl. Phys. **A642**, 387 (1998)
- [4] K. Hara and Y. Sun, Int. J. Mod. Phys. **E4**, 637 (1995)
- [5] T. Bengtsson and I. Ragnarsson, Nucl. Phys. **A436**, 14 (1985)
- [6] M. Dufour and A.P. Zuker, Phys. Rev. **C54**, 1641 (1996)
- [7] W. Dieterich, A. Bäcklin, C.O. Lannergård, and I. Ragnarsson, Nucl. Phys. **A253**, 429 (1975)
- [8] T. Mizusaki, T. Otsuka, Y. Utsuno, M. Homma and T. Sebe, to be published in Phys. Rev. **C**, Rapid Communication (1999)
- [9] K. Hara and Y. Sun, Nucl. Phys. **A529**, 445 (1991)
- [10] T. Tanaka, K. Iwasawa and F. Sakata, Phys. Rev. **C58**, 2765 (1998)
- [11] K. Hara and Y. Sun, unpublished (1996)

FIG. 1.

The γ -ray transition energies $E_\gamma(I) = E(I) - E(I - 2)$ as functions of spin. The experimental data is taken from Ref. [3] and the result of pf-SM from Ref. [1]. PSM and GCM are the results of the present work.

FIG. 2. The $B(E2)$ values as functions of spin. The experimental data are taken from Ref. [3] and the result of pf-SM from Ref. [1]. PSM and GCM are the results of the present work.

FIG. 3. Band diagram of the PSM

FIG. 4. Band diagram of the GCM

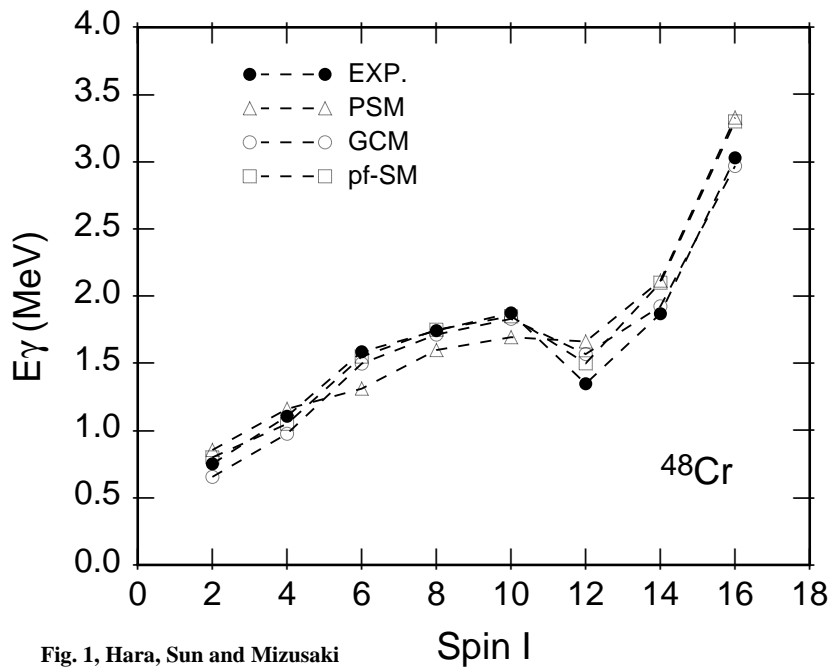


Fig. 1, Hara, Sun and Mizusaki Spin I

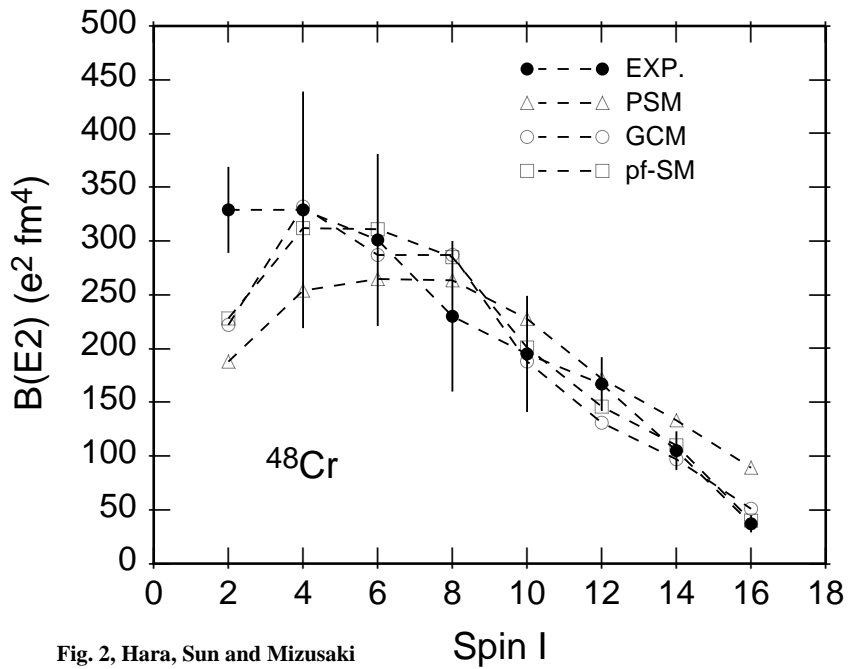


Fig. 2, Hara, Sun and Mizusaki Spin I

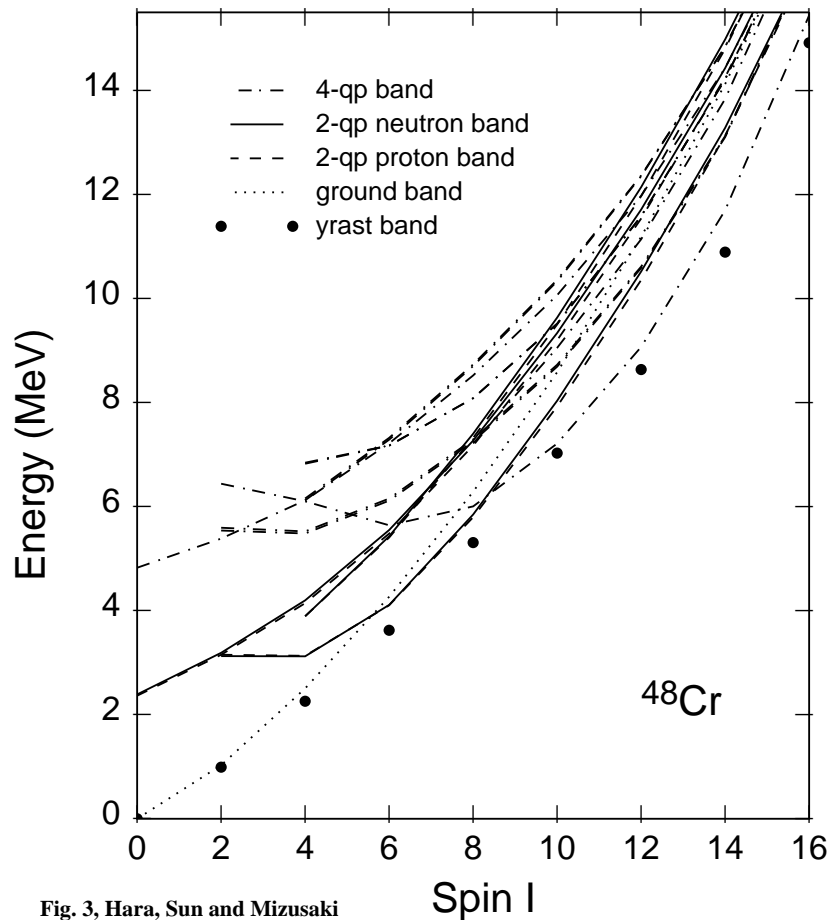


Fig. 3, Hara, Sun and Mizusaki

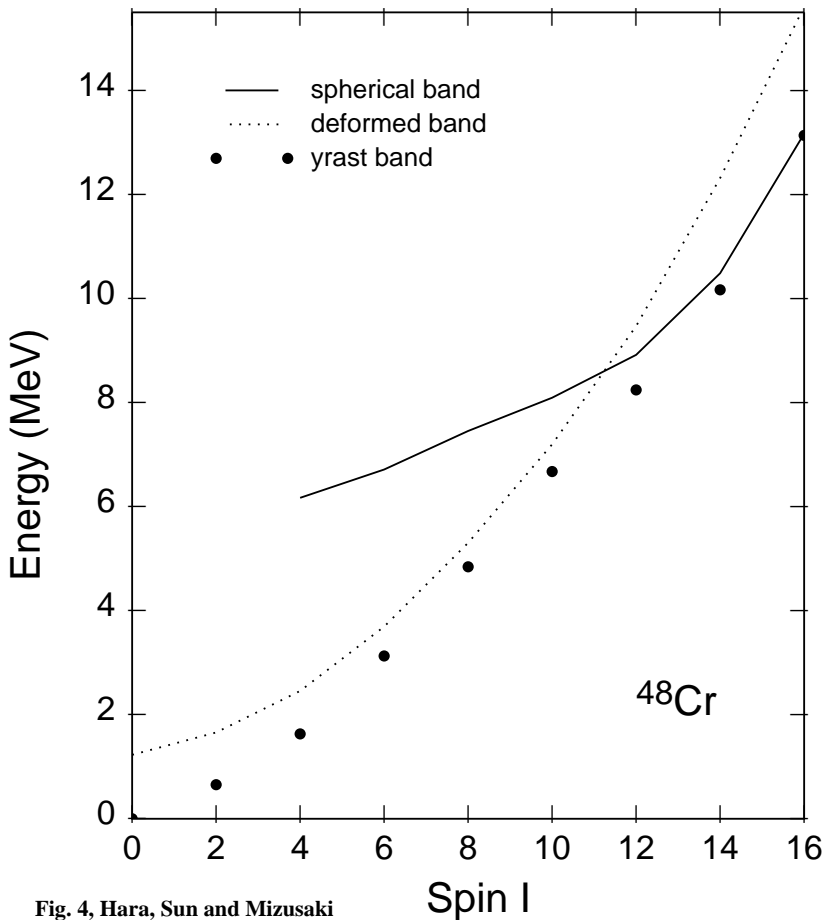


Fig. 4, Hara, Sun and Mizusaki